Gain-Scheduled Higher Harmonic Control for Full Flight Envelope Vibration Reduction

Gain-Scheduled Higher Harmonic Control for Full Flight Envelope Vibration Reduction

Frank H. Fan
frankhfan@gmail.com
Engineer
Japan Agency for Marine-Earth Science and Technology
Yokohama, Japan

Steven R. Hall
srhall@mit.edu
Professor of Aeronautics and Astronautics
Massachusetts Institute of Technology
Cambridge, MA, USA

ABSTRACT

This paper investigates the dynamics of the SMART rotor, and presents a method to design a gain-scheduled controller to reduce the harmonic vibration throughout the flight envelope. The dynamics of the SMART rotor was examined at various flight conditions through nonlinear simulation. The simulation results showed that the dynamics is strongly dependent on the advance ratio, but only weakly dependent on the blade loading and the rotor shaft angle. To reduce the higher harmonic vibration throughout the flight envelope, a controller gain-scheduled on the advance ratio is presented. Output from linear time-invariant higher harmonic controllers designed for different flight conditions are blended to form the gain-scheduled controller. Closed-loop simulations of the helicopter rotor undergoing transitional flight with increasing advance ratio were conducted. The results from the closed-loop simulations show that the 5 per rev normal vibration was reduced by over 97% at the rotor hub.

INTRODUCTION

The asymmetric loading on the main rotor in forward flight produces periodic forces and moments in the helicopter rotor. The vibratory forces and moments are transmitted from the rotor hub to the fuselage, resulting in higher harmonic vibration that is problematic in many ways. The vibration reduces the passenger and pilot comfort level, induces fatigue in the structural components, thus increasing the maintenance cost, and reduces the effectiveness of onboard equipment. Although there are other sources of vibration in a helicopter, the reduction of vibration caused by the main rotor has been the focus of research on helicopter vibration reduction (Ref. 15).

Helicopter vibration can be reduced through the use of either passive vibration reduction methods (Ref. 19) or active control methods (Ref. 5). Passive vibration reduction methods reduce the effects of the vibration with the application of vibration absorbers and vibration isolation systems (Ref. 12). The passive methods are widely used, but they are generally heavy and cannot adapt to changes in flight condition (Ref. 18). Active helicopter vibration control methods, generally referred to as higher harmonic control (HHC), typically use some form of actuation on the rotor blades to modify the lift forces in order to reduce the periodic forces and moments at the helicopter rotor hub.

The seminal work on HHC by Shaw (Ref. 20), and McHugh and Shaw (Ref. 16) explored the use of swashplate to generate the feathering motion of the rotor blades in order to reduce the higher harmonic vibratory forces at the rotor hub. Subsequent work by Shaw (Ref. 21), and Shaw and Albion (Ref. 22) further developed the control algorithm aspect of HHC. Johnson (Ref. 13) provided a detailed discussion on different approaches to implement the HHC algorithm, including the use of recursive parameter estimation to ensure the controller can reduce vibration at different flight conditions. The effectiveness of HHC has been shown through windtunnel tests (Refs. 17, 23) and flight tests (Ref. 26). Various means of actuation other than the swashplate have been considered, including discretely actuated trailing edge flaps on the rotor blades (Ref. 9), and controlling the pitch angle of the individual rotor blades (Ref. 11).

The HHC algorithm developed by Shaw and McHugh is a discrete-time controller based on a linear quasisteady model of the helicopter rotor. Hall and Wereley (Ref. 10) showed that the discrete-time HHC can be implemented with a demodulation/modulation scheme, resulting in a continuous-time version of the HHC. The continuous-time controller is similar to the classical controller for narrow-band disturbance rejection (Ref. 25), and the HHC algorithm can be interpreted as an instance of the internal model principle (Ref. 4). Gupta, Du Val and Gregory (Refs. 1, 6, 7) used a linear time-invariant (LTI) plant model to represent the helicopter, and designed a controller using a frequency weighted version of the linear-quadratic-Gaussian (LQG) method. The frequency weighting was provided by an undamped second-order oscillator with a natural frequency tuned to N/rev, where N is the number of rotor blades. Fan and Hall (Ref. 3) introduced an extension of the continuous-time HHC algorithm, in which a fixed-order $\mathscr{H}_\infty$ controller was designed for an LTI plant model representing the helicopter rotor at a particular flight condition. A notch

Presented at the AHS 70th Annual Forum, Montréal, Québec, Canada, May 20–22, 2014.

filter with transmission zeros at the harmonic frequencies was used to generated the fixed-order $\mathscr{H}_\infty$ controller. The shape of the notch filter provides the definitions for two metrics, peak sensitivity $S_{\max}$ and bandwidth ω_B, that quantify the performance of the controller for harmonic disturbance rejection.

The dynamics of a helicopter is inherently periodic due to the operation of the main rotor, although for some rotors, including the Smart Material Actuated Rotor Technology (SMART) rotor (Ref. 8) examined in this paper, the effect of periodic dynamics is small (Refs. 3, 24). The negligible amount of periodicity justifies the use of an LTI model to describe the dynamics at a specific flight condition. However, there is significant variation of the helicopter dynamics with respect to the flight condition. Thus the harmonic disturbance rejection controller must be able to accommodate the variation in helicopter rotor dynamics at different flight conditions.

In this paper, we first examine the variation of the SMART helicopter rotor dynamics through simulation conducted at different flight conditions. Then we present a method to design a controller to reduce the vibration in a helicopter throughout the entire flight envelope. The full flight envelope controller is a gain-scheduled controller based on fixed-order $\mathscr{H}_\infty$ controllers designed for different flight conditions. The gain-scheduling is accomplished by blending the output of the fixed-order $\mathscr{H}_\infty$ controllers based on the value of the advance ratio μ. The performance of the gain-scheduled controller is demonstrated through closed-loop CAMRAD simulation, with open-loop simulation results used as the baseline to gauge the effectiveness of the gain-scheduled controller.

SMART ROTOR DYNAMICS AT DIFFERENT FLIGHT CONDITIONS

The SMART rotor is a 5-bladed rotor with an independent active partial span trailing edge flap on each rotor blade. At a constant flight condition, the dynamics of the SMART rotor is only weakly periodic, thus enabling us to use transfer function to describe its dynamics. For our purpose, the transfer function describes the linearized input to output relationship between the collective command and the normal rotor hub vibratory force. The collective command is represented by the common angular displacement of the trailing edge flaps.

SMART Rotor Transfer Functions

The transfer functions of the SMART rotor at different flight conditions were estimated using results from CAMRAD simulations. The estimated transfer function contains the input to output relationship of the rotor at discrete frequencies, and is referred to as the empirical transfer function estimate (ETFE). The ETFEs were used for two purposes. First, they were used to determine the effects of flight condition on the rotor dynamics. Second, they were used to generate the parametric models needed for the control design process. The parametric models of the helicopter rotor at different flight conditions, in the form of rational transfer functions, were obtained from the ETFEs using techniques from system identification (Ref. 14).

Table 1: Flight conditions used in CAMRAD simulations

μ	α (deg)	C_T/σ
0.15	-10.0	0.075
0.15	7.0	0.075
0.15	-3.7	0.075
0.15	-3.7	0.090
0.15	-10.0	0.040
0.15	-3.7	0.040
0.20	2.0	0.075
0.20	-5.5	0.075
0.20	-5.5	0.040
0.20	-5.5	0.090
0.20	-10.0	0.075
0.30	-9.1	0.040
0.30	-9.1	0.075
0.30	-9.1	0.090
0.30	-15.0	0.040
0.30	-15.0	0.070
0.30	-5.0	0.040
0.30	-5.0	0.100
0.375	-12.0	0.075
0.375	-12.0	0.040
0.375	-12.0	0.065

Table 2: Segments of the linear sinusoidal sweep input signal used in CAMRAD simulations

Segment	1	2	3	4
Starting frequency (Hz)	0.0	18.7	38.7	58.7
Ending frequency (Hz)	21.307	41.3	61.3	79.998
Duration of sweep (sec)	21.308	22.6	22.6	21.299

CAMRAD simulations were conducted for 21 different flight conditions, and the results were analyzed to help us understand the SMART rotor dynamics throughout the flight envelope. The flight conditions with different combinations of the advance ratio μ, rotor shaft angle α, and blade loading coefficient C_T/σ used in the simulations are shown in Table 1.

For the purpose of identifying the dynamics of the SMART rotor, the simulations were performed with a linear sinusoidal sweep collective command driving the trailing edge flaps. Due to computer hardware limitation and data resolution requirement, the collective command provided to the flaps for each flight condition was divided into four segments as shown in Table 2. For each segment, the amplitude of the linear sinusoidal sweep was 1 deg, and the input signal started at 1 second into the simulation. The total duration of each individual segment was 24.6 seconds. The overlaps in the starting and ending frequencies between the segments ensure the input signal contained enough power to properly excite the system in the entire frequency range of interest, which is from 0 per rev up to approximately 12 per rev. A constant rotor frequency of $\Omega = 392$ rpm was used in the CAMRAD simulation, and both the input and output data were generated at a time interval of 0.001 sec.

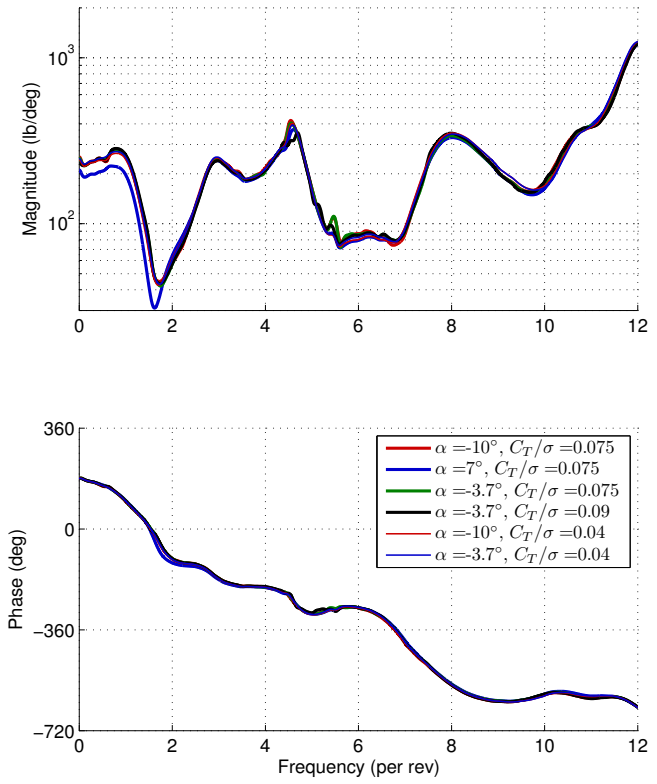

Fig. 1: Transfer functions of the SMART rotor obtained from CAMRAD simulation results, with $\mu = 0.15$

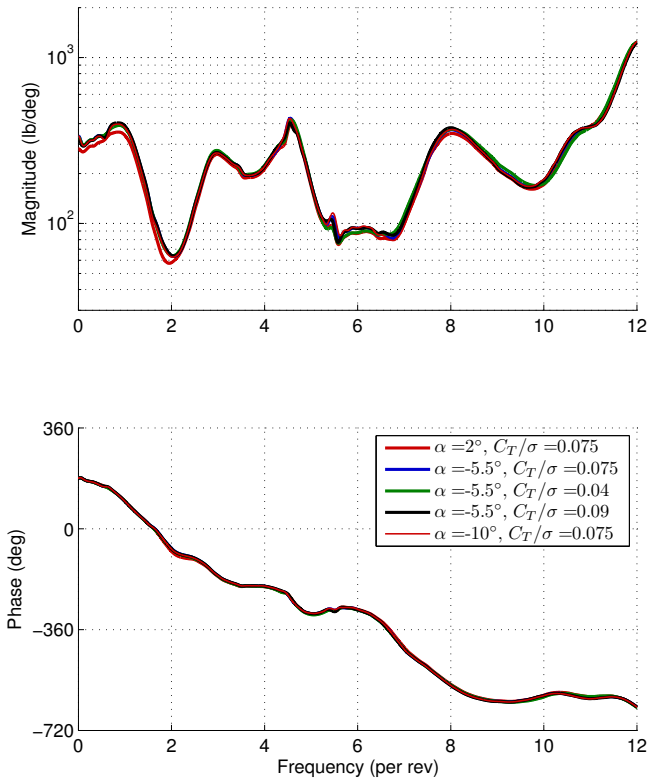

Fig. 2: Transfer functions of the SMART rotor obtained from CAMRAD simulation results, with $\mu = 0.20$

An estimate of the transfer function was generated from the simulation results for each flight condition listed in Table 1. The empirical transfer function estimates were obtained as the ratio between the autospectral density of the input and the cross-spectral density of the input and output. See Reference 3 for further details on obtaining the empirical transfer function estimate. The transfer functions of the SMART rotor obtained from the CAMRAD simulations are shown in Figures 1, 2, 3, and 4. For each figure, the transfer functions represent the SMART rotor dynamics at flight conditions with the same value of the advance ratio μ, but different combinations of rotor shaft angle α and blade loading coefficient C_T/σ. Qualitative comparison of the transfer functions shows that the dynamics of the helicopter rotor is only weakly dependent on the rotor shaft angle α and blade loading coefficient C_T/σ. However, the magnitude of the transfer functions increases substantially with increasing value of the advance ratio μ. The examination of the magnitude of the transfer functions shows that the SMART rotor dynamics are insensitive to change in the rotor shaft angle and blade loading coefficient, and sensitive to changes in the advance ratio. The implication is that an effective harmonic disturbance rejection controller for the entire flight envelope must take in account the variation in dynamics due to the change in μ.

SMART Rotor Parametric Models

Parametric models of the SMART helicopter rotor are needed in order to design controllers for effective harmonic disturbance rejection. For each flight condition, the parametric

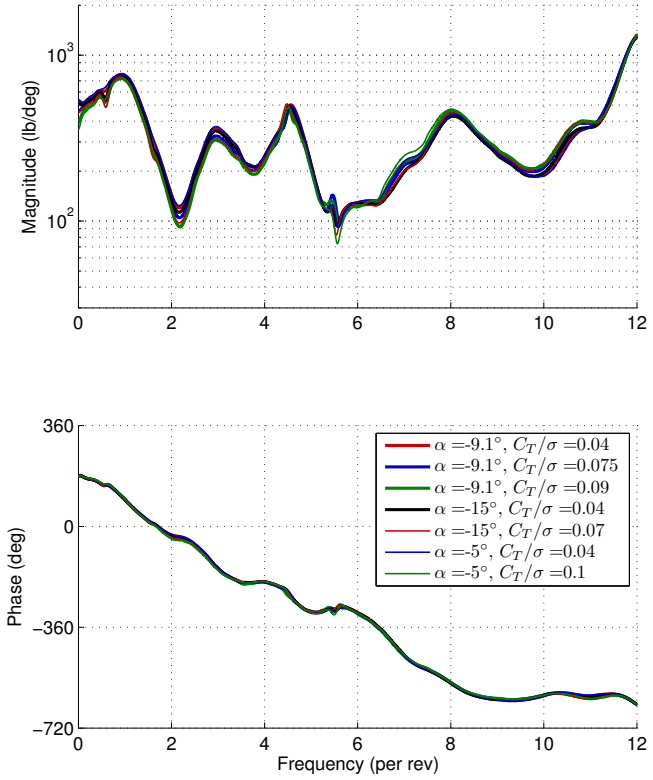

Fig. 3: Transfer functions of the SMART rotor obtained from CAMRAD simulation results, with $\mu = 0.30$

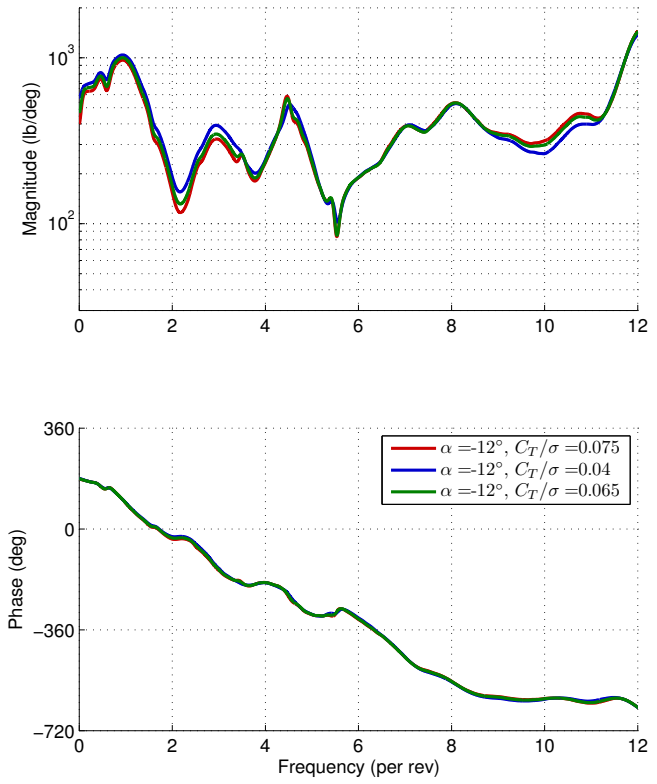

Fig. 4: Transfer functions of the SMART rotor obtained from CAMRAD simulation results, with $\mu = 0.375$

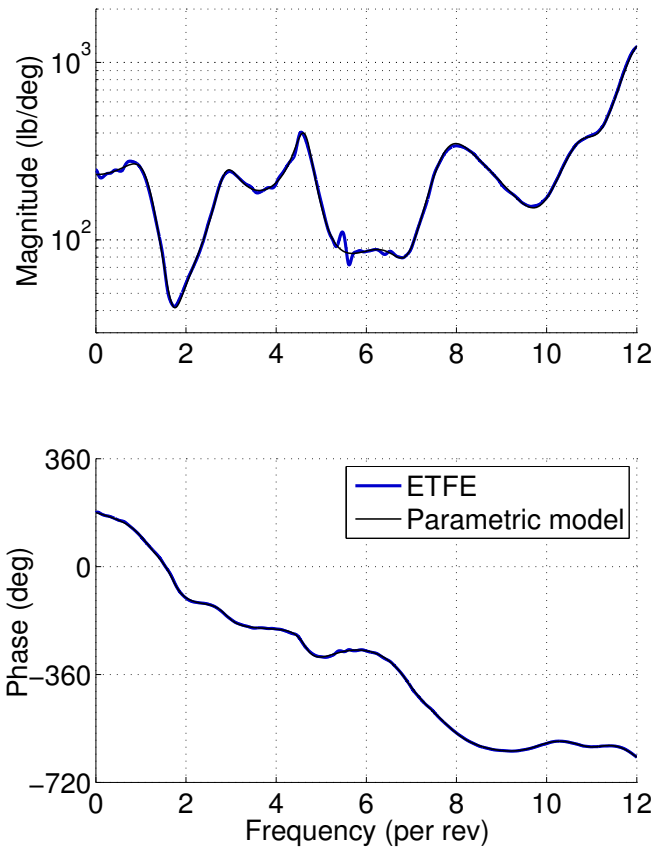

Fig. 5: Comparison between the empirical transfer function estimate and the parametric model of the SMART rotor at $\mu = 0.15$, $\alpha = -3.7°$, $C_T/\sigma = 0.075$

model is represented by a rational transfer function $\widehat{G}(j\omega;\theta)$. The unknown coefficients of the rational transfer function, denoted by θ, were obtained by minimizing the weighted magnitude of the output error E between the simulation output and the predicted output. The output error is defined as

$$E(j\omega;\theta) = Y(j\omega) - \widehat{G}(j\omega;\theta)U(j\omega) \tag{1}$$

where U and Y are, respectively, the Fourier transforms of the collective input command and the hub normal force output from the CAMRAD simulation. We used the inverse of the magnitude of the empirical transfer function estimate as the weighting function. This choice of weighting function places emphasis at the frequency ranges where the system response is low, which ensures that the transmission zeros are well represented by the rational transfer function. Details on the procedure to obtain the rational transfer function from the simulation data can be found in Reference 2.

Four representative parametric models of the SMART rotor, one for each value of the advance ratio μ used in the CAMRAD simulations, are shown in Figures 5, 6, 7, and 8. For each figure, the empirical transfer function estimate at the same flight condition is also shown for comparison purpose. The identified rational transfer functions closely approximate the corresponding empirical transfer function estimates, and were subsequently used for controller design.

HARMONIC DISTURBANCE REJECTION FOR MULTIPLE PLANTS

The transfer function obtained from the CAMRAD simulations show that there is significant variation in the SMART rotor dynamics with respect to change in μ. For effective vibration reduction throughout the flight envelope, the controller must explicitly account for the large change in the rotor dynamics as μ varies. However, even at a fixed μ, there are some minor variations in the dynamics as α and C_T/σ are varied. In this section, we provide a modified version of the fixed-order $\mathscr{H}_\infty$ controller to account for the small variations in the rotor dynamics with respect to changes in both α and C_T/σ, while μ is kept constant.

Harmonic Disturbance Rejection Performance

The fixed-order $\mathscr{H}_\infty$ control synthesis method of Reference 3 casts the helicopter vibration reduction problem as an output disturbance rejection problem within the $\mathscr{H}_\infty$ framework. The block diagram in Figure 9 shows the $\mathscr{H}_\infty$ analysis setup used to determine the performance of the controller $K(s)$. The helicopter rotor plant is denoted by $G(s)$, $W(s)$ is a weighting filter for quantifying the controller performance, and the higher harmonic vibration is modeled as the output disturbance d. The sensitivity function $S(s)$, which is the closed-loop trans-

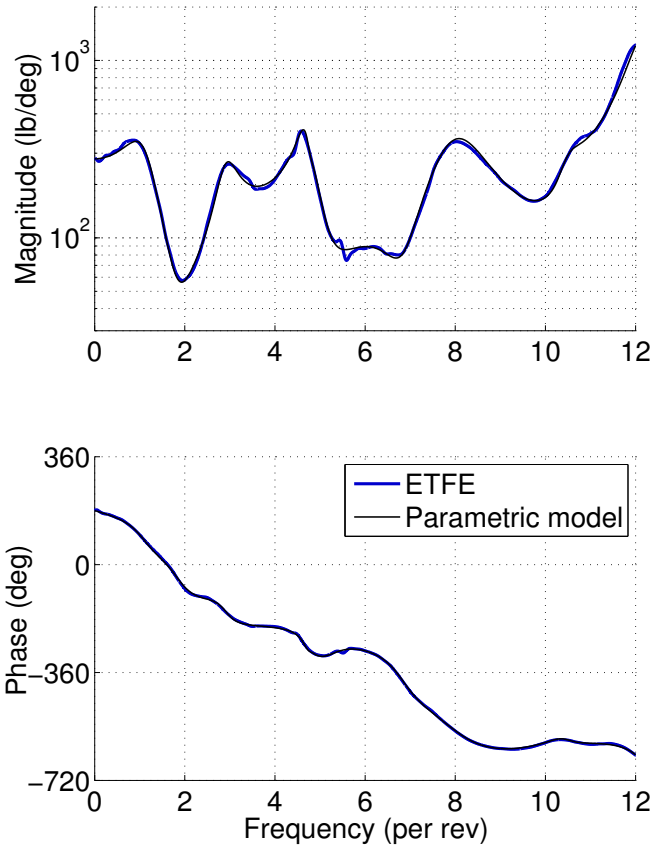

Fig. 6: Comparison between the empirical transfer function estimate and the parametric model of the SMART rotor at $\mu = 0.20$, $\alpha = 2.0°$, $C_T/\sigma = 0.075$

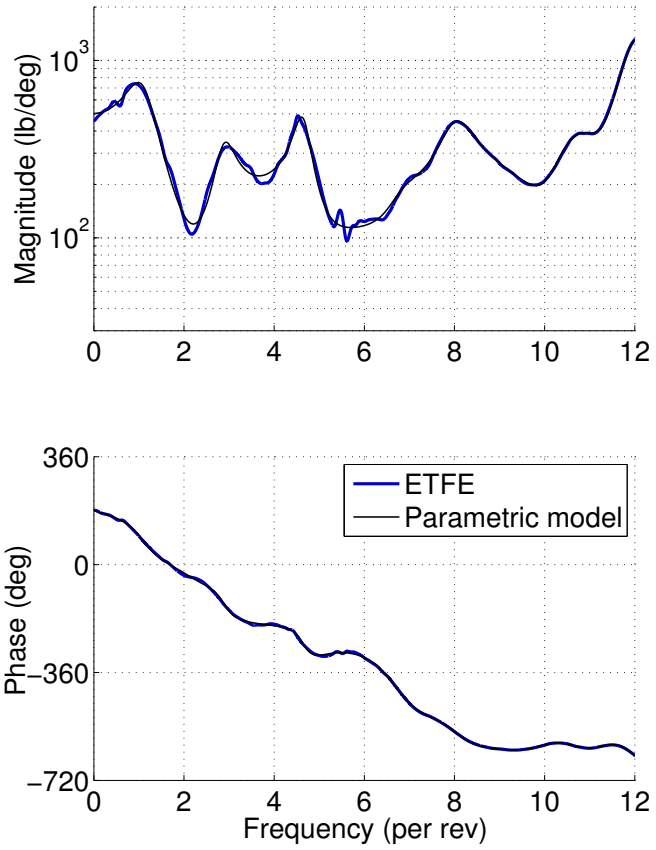

Fig. 7: Comparison between the empirical transfer function estimate and the parametric model of the SMART rotor at $\mu = 0.30$, $\alpha = -9.1°$, $C_T/\sigma = 0.075$

fer function from the disturbance d to the output y, is given by

$$S(s) = (1 - G(s)K(s))^{-1} \tag{2}$$

A notch in the sensitivity function at the harmonic frequency is necessary to reject the harmonic disturbance. The bandwidth ω_B and peak sensitivity $S_{\max}$ are defined by the magnitude of the ideal notch filter $\mathscr{V}$ as shown in Figure 10. For rejection of disturbance at multiple harmonics, a notch is needed at each harmonic frequency to be attenuated.

In the $\mathscr{H}_\infty$ framework, the weighting filter $W(s)$ must be a rational transfer function. The ideal notch filter is used to generate the weighting filter $W(s)$ through the relationship

$$W(s) \approx \mathscr{V}^{-1}(s) \tag{3}$$

The bandwidth and peak sensitivity of a given controller is determined by checking whether the weighted sensitivity function satisfies the inequality

$$\|W(s)S(s)\|_\infty \leq 1 \tag{4}$$

Bandwidth and peak sensitivity are both performance measures of the higher harmonic controller. A larger bandwidth allows the controller to respond faster to changes in the harmonic disturbance; a lower peak sensitivity corresponds to higher gain and phase margins, resulting in greater robustness. The fixed-order $\mathscr{H}_\infty$ control method is used to obtain a controller that is pareto optimal in terms of the bandwidth and peak sensitivity. Typically, the peak sensitivity is chosen to be 1.2, which translates to a gain margin of at least 6, and a phase margin of at least 49.2 deg. Increasing the value of peak sensitivity would lead to a larger bandwidth, but the gain margin and phase margin would be reduced.

Fixed-Order $\mathscr{H}_\infty$ Controller for Multiple Plants

The fixed-order $\mathscr{H}_\infty$ control synthesis method is only applicable to a single LTI model. Thus the fixed-order $\mathscr{H}_\infty$ controller is only intended to attenuate the higher harmonic vibration at one flight condition. To address the slight differences in the plant dynamics due to variations in α and C_T/σ, a simple modification was made to the cost function used in the synthesis of the fixed-order $\mathscr{H}_\infty$ controller. The modification ensures the fixed-order controller designed for a specific μ will have adequate performance for that particular value of μ, regardless of the values of α and C_T/σ.

Denoting the parametric rotor models at a specific advance ratio by $G_k(s)$, $k = 1,2,...,N_m$, the objective of a single controller $K(s)$ for multiple plant models is to achieve pareto optimality in terms of maximizing the bandwidth while minimizing the peak sensitivity in all of the sensitivity functions $S_k(s)$, with $S_k(s)$ given by

$$S_k(s) = (1 - G_k(s)K(s))^{-1}, \quad k = 1,2,...,N_m \tag{5}$$

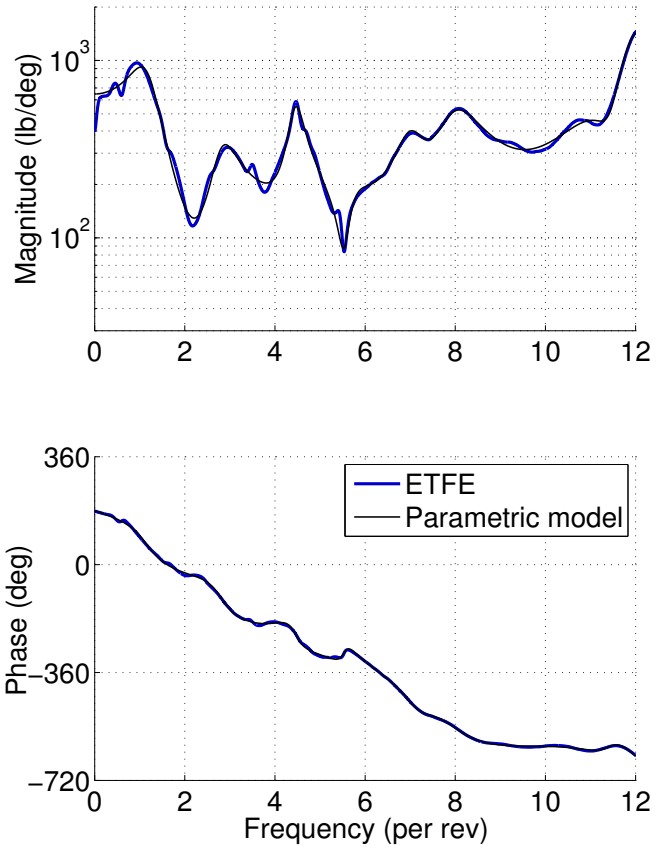

Fig. 8: Comparison between the empirical transfer function estimate and the parametric model of the SMART rotor at $\mu = 0.375$, $\alpha = -12.0°$, $C_T/\sigma = 0.075$

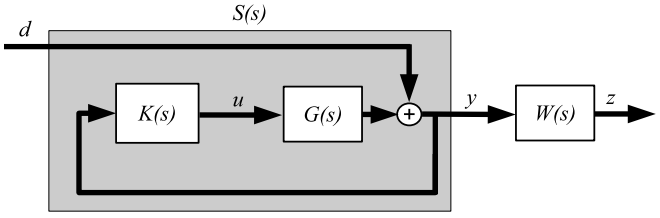

Fig. 9: Block diagram for performance analysis

The bandwidth ω_B and peak sensitivity $S_{\max}$ achieved by the single controller $K(s)$ is quantified by a single weighting filter $W(s)$ for all plant models, which can be expressed as

$$\|W(s)S_k(s)\| \leq 1, \quad \forall k \tag{6}$$

The controller $K(s)$ is obtained by modifying the fixed-order $\mathscr{H}_\infty$ control synthesis procedure by making the following modification to the cost function

$$J = \sum_{k=1}^{N_m} J_k \tag{7}$$

where J_K is the fixed-order $\mathscr{H}_\infty$ synthesis cost function for the plant $G_k(s)$ with weighting filter $W(s)$, and controller $K(s)$. The gradient of the cost function J, which is used in the optimization to obtain the controller, is similarly modified as

$$\frac{\partial J}{\partial \theta} = \sum_{k=1}^{N_m} \frac{\partial J_k}{\partial \theta} \tag{8}$$

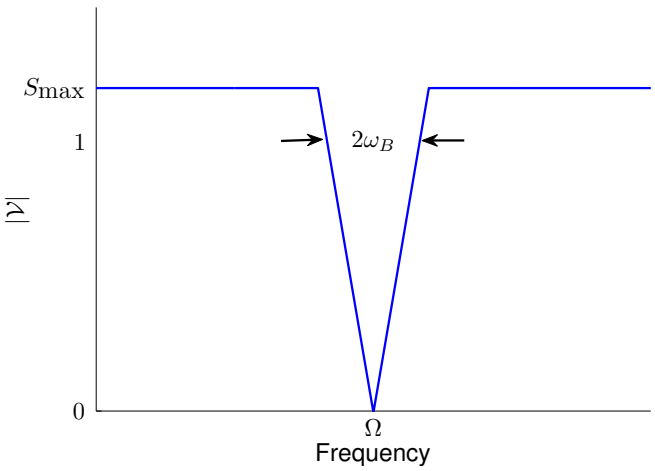

Fig. 10: Magnitude of the ideal notch filter with definitions of bandwidth ω_B and peak sensitivity $S_{\max}$

An initial feasible controller is necessary to generate the initial parameter vector θ required to start the optimization. We obtained the initial parameters from a continuous-time higher harmonic controller designed using the method of Hall and Wereley (Ref. 10). The optimization procedure then proceeds as discussed in Reference 3.

The feasibility of the control problem can be determined from the phase of the plants at the harmonic frequencies to be attenuated. Since HHC can be interpreted as phase stabilization at the frequencies of the harmonic disturbance, the phases of all the plant models at these harmonic frequencies must be within a 180° sector. However, feasibility does not imply any performance guarantee, and the performance of the single fixed-order $\mathscr{H}_\infty$ controller would degrade with larger variation in the phases at the harmonic frequencies.

GAIN-SCHEDULED HARMONIC DISTURBANCE REJECTION CONTROLLER

In the previous section, we provided a method to design a harmonic disturbance rejection controller to account for the slight variations in the plant dynamics due to variations in α and C_T/σ at a fixed value of μ. The fixed-order $\mathscr{H}_\infty$ controllers $K_j(s)$, $j = 1,2,...,M$, designed for specific value of the advance ratios $\mu = \mu_j$, $j = 1,2,...,M$, are used in this section to construct a gain-scheduled controller for harmonic disturbance rejection throughout the flight envelope. M represents the number of models used to span the advance ratio in the flight envelope.

The block diagram of the gain-scheduled feedback control system is shown in Figure 11. In addition to the hub normal force y, the controller also requires the value of the advance ratio μ. The inherent structure of the continuous-time higher harmonic controller contained within the fixed-order $\mathscr{H}_\infty$ controller provides a decomposition suitable for controller scheduling. The same controller decomposition also allows the implementation of the demodulation/modulation

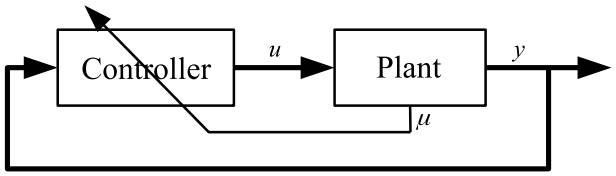

Fig. 11: Feedback structure for gain-scheduled controller

scheme developed by Hall and Wereley (Ref. 10), and the associated anti-windup algorithm developed by Shin, Cesnik, and Hall (Ref. 24). The demodulation/modulation scheme is not used in this paper, since the validation work performed for this paper were done using CAMRAD simulations with constant rotor speed. However, the demodulation/modulation implementation is necessary in the case that azimuthal position of the rotor is used as the independent variable in the controller synthesis procedure. The benefit of using the azimuthal position as the independent variable is that by doing so, the frequency of the controller poles on the $j\omega$-axis (i.e. the frequency at which disturbances are rejected) automatically changes to track the rotor frequency, and therefore the frequency of the disturbances.

Controller Blending

The scheduling of the controller is achieved by blending the outputs of the fixed-order $\mathscr{H}_\infty$ controllers based on the value of μ. For the current value of μ, with $\mu_j \le \mu < \mu_{j+1}$, the control signal from the gain-scheduled controller is obtained as

$$U(s;\mu) = (1-\alpha(\mu))U_j(s) + \alpha(\mu)U_{j+1}(s) \tag{9}$$

where $U_j(s)$ is the output of the controller $K_j(s)$ designed for $\mu = \mu_j$, $U_{j+1}(s)$ is the output of the controller $K_{j+1}(s)$ designed for $\mu = \mu_{j+1}$, and we used a blending function $\alpha(\mu)$ given by

$$\alpha(\mu) = \frac{\mu - \mu_j}{\mu_{j+1} - \mu_j}, \quad \mu_j \le \mu < \mu_{j+1} \tag{10}$$

Our choice of using a linear $\alpha(\mu)$ in Equation (9) results in linear interpolation of the control signal, satisfying the boundary conditions

$$\begin{aligned} U(s;\mu_j) &= U_j(s) \\ U(s;\mu_{j+1}) &= U_{j+1}(s) \end{aligned} \tag{11}$$

It is possible to use other types of blending function that satisfy Equation (11).

When the value of μ in Equation (9) moves out of the interval $[\mu_j,\ \mu_{j+1})$, another control signal must be available for the blending of the controller output to continue. Instead of switching on the individual controller $K_{j-1}(s)$ or $K_{j+2}(s)$ as needed, we keep all individual controllers online and blend their control signals. In the case that fixed-order $\mathscr{H}_\infty$ controllers $K_j(s)$ are designed for M different values of the advance ratio μ_j, $j = 1,2,...,M$, the controller blending rule is

$$U(s;\mu) = \sum_{j=1}^{M} \alpha_j(\mu)U_j(s) \tag{12}$$

where the blending functions $\alpha_j,\ j = 1,2,...,M$, are given by

$$\alpha_1(\mu) = \begin{cases} 1 & \mu < \mu_1 \\ \frac{\mu_2-\mu}{\mu_2-\mu_1} & \mu_1 \le \mu < \mu_2 \\ 0 & \mu > \mu_2 \end{cases} \tag{13}$$

$$\alpha_j(\mu) = \begin{cases} 0 & \mu < \mu_{j-1} \\ \frac{\mu-\mu_{j-1}}{\mu_j-\mu_{j-1}} & \mu_{j-1} \le \mu < \mu_j \\ \frac{\mu_{j+1}-\mu}{\mu_{j+1}-\mu_j} & \mu_j \le \mu < \mu_{j+1} \\ 0 & \mu \ge \mu_{j+1} \end{cases} \tag{14}$$

$$\alpha_M(\mu) = \begin{cases} 0 & \mu < \mu_M - 1 \\ \frac{\mu-\mu_{M-1}}{\mu_M-\mu_{M-1}} & \mu_{M-1} \le \mu < \mu_M \\ 1 & \mu \ge \mu_M \end{cases} \tag{15}$$

The blending of all the available individual fixed-order $\mathscr{H}_\infty$ controllers ensures the control signal remains continuous. The continuous control signal results in smooth transitions, i.e. bumpless transfers, as the advance ratio varies between the different intervals of μ during operation. A drawback of the controller blending scheme is that all of the fixed-order $\mathscr{H}_\infty$ controllers are always online. Keeping the fixed-order $\mathscr{H}_\infty$ controllers that are not contributing to the control signal increases the order of the gain-scheduled controller. However, the common harmonic poles of the fixed-order $\mathscr{H}_\infty$ controllers provides a structure that can be used to lessen the increase in controller order.

Structure of the Gain-Scheduled Controller

The construction of the fixed-order $\mathscr{H}_\infty$ controller consists of a dynamic filter in parallel with a harmonic disturbance rejection filter. For the purpose of implementation in the gain-scheduled controller, the fixed-order $\mathscr{H}_\infty$ controllers for $\mu = \mu_j$, $j = 1,2,...,M$, are decomposed in series as

$$K_j(s) = \frac{B_j(s)}{A_j(s)} = \frac{B_{h_j}(s)}{A_{h_j}(s)}\frac{B_{d_j}(s)}{A_{d_j}(s)} = K_{h_j}(s)K_{d_j}(s),\ j = 1,2,...,M \tag{16}$$

where

$$K_{h_j}(s) = \frac{B_{h_j}(s)}{A_{h_j}(s)} \tag{17}$$

is the serial harmonic disturbance rejection filter, and

$$K_{d_j}(s) = \frac{B_{d_j}(s)}{A_{d_j}(s)} \tag{18}$$

is the serial dynamic filter. $K_{h_j}(s)$ contains all the $j\omega$-axis poles of $K_j(s)$ corresponding to the frequencies of the harmonic disturbance to be attenuated. $K_{d_j}(s)$ contains the remaining poles of $K_j(s)$. The zeros of $K_{h_j}(s)$ and $K_{d_j}(s)$ are selected so that the polynomials $B_{h_j}(s)$ and $B_{d_j}(s)$ have real coefficients. Additionally, $K_{h_j}(s)$ is chosen to be strictly proper, with the general form

$$K_{h_j}(s) = \sum_{i=1}^{N} \frac{a_{ij}s + b_{ij}n_i\Omega}{s^2 + (n_i\Omega)^2},\ j = 1,2,...,M \tag{19}$$

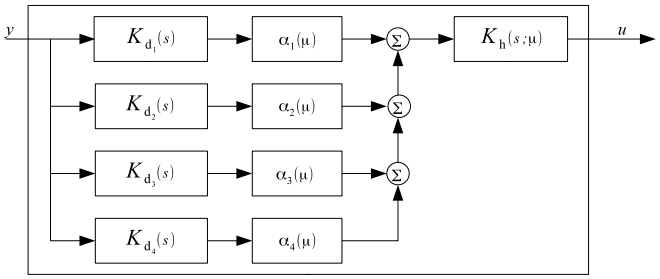

Fig. 12: Block diagram for the implementation of the gain-scheduled controller

where n_i, $i = 1,2,...,N$, are integers representing the harmonics to be attenuated. $K_{h_j}(s)$ as shown in Equation (19) has the same form as the continuous-time HHC of Hall and Wereley, thus the demodulation/modulation scheme of Reference (Ref. 10) and the anti-windup scheme of Reference (Ref. 24) can both be applied to the gain-scheduled controller.

The state-space realizations of $K_{h_j}(s)$ can be obtained from the transfer function in Equation (19) as

$$K_{h_j}(s) \sim \left(\begin{array}{c|c} A_h & B_{h_j} \\ \hline C_h & 0 \end{array} \right) \tag{20}$$

where A_h is a block diagonal matrix with 2×2 matrices of the form

$$\begin{bmatrix} 0 & n_i\Omega \\ -n_i\Omega & 0 \end{bmatrix} \tag{21}$$

along the diagonal, and

$$B_{h_j} = \begin{bmatrix} a_{1j} & b_{1j} & a_{2j} & b_{2j} & \cdots & a_{Nj} & b_{Nj} \end{bmatrix}^T \tag{22}$$

$$C_h = \begin{bmatrix} 1 & 0 & 1 & 0 & \cdots & 1 & 0 \end{bmatrix} \tag{23}$$

Since the disturbance rejection filters $K_{h_j}(s)$, $j = 1,2,...,M$, all have the same state-space matrices A_h and C_h, they can be replaced by a single gain-scheduled disturbance rejection filter with the state-space realization

$$K_h(s;\mu) \sim \left(\begin{array}{c|c} A_h & B_h(\mu) \\ \hline C_h & 0 \end{array} \right) \tag{24}$$

with the matrix $B_h(\mu)$ given by

$$B_h(\mu) = \begin{bmatrix} a_1(\mu) & b_1(\mu) & \cdots & a_N(\mu) & b_N(\mu) \end{bmatrix}^T \tag{25}$$

where

$$a_i(\mu) = \sum_{j=1}^{M} \alpha_j(\mu) a_{ij},\ i = 1,2,...,N \tag{26}$$

$$b_i(\mu) = \sum_{j=1}^{M} \alpha_j(\mu) b_{ij},\ i = 1,2,...,N \tag{27}$$

The implementation of the gain-scheduled controller is shown as a block diagram in Figure 12.

In this section, we outlined the procedure for obtaining a harmonic disturbance rejection controller for the entire flight envelope. In our case, the variation in the dynamics is captured by the advance ratio μ. Thus the controller is gain-scheduled on just a single variable using linear blending functions. The procedure can be extended to gain-scheduling on multiple variables with appropriate modification to the blending functions. For harmonic disturbance rejection, the harmonic poles of the individual fixed-order $\mathscr{H}_\infty$ controllers do not have to be duplicated in the controller blending scheme. The result is that our gain-scheduled harmonic disturbance rejection controller is of lower order than simply blending the output of all the fixed-order $\mathscr{H}_\infty$ controllers.

CLOSED-LOOP SIMULATION

The gain-scheduled harmonic disturbance rejection control method is demonstrated with a controller designed for the SMART rotor. The performance of the controller is evaluated through closed-loop simulations. Baseline levels of vibration were obtained by running the simulations in open-loop, which was accomplished by disconnecting the gain-scheduled controller output from the helicopter rotor model. Both the open-loop and closed-loop simulations were conducted in CAMRAD using flight profiles with increasing advance ratio. The model used in the controller validation simulations is the same SMART rotor model used for plant identification, with the hub normal force used as the feedback signal.

Closed-Loop Simulation Setup

The rational transfer functions obtained from the SMART rotor dynamics identification simulations were used as the plant models in the control design process. In our case, we used four values of the advance ratio, $\mu_1 = 0.15$, $\mu_2 = 0.2$, $\mu_3 = 0.3$, and $\mu_4 = 0.375$, to span the entire flight envelope. Thus the gain-scheduled controller is constructed from four fixed-order $\mathscr{H}_\infty$ controllers, one for each specific value of μ. Each of the four fixed-order $\mathscr{H}_\infty$ controllers were designed to reject the normal vibration at the first five harmonic frequencies. We did not incorporate the additional dynamic filter, denoted by $K_{d_j}(s)$ in Equation (16), so each fixed-order $\mathscr{H}_\infty$ controller is 10th order. The four fixed-order $\mathscr{H}_\infty$ controllers are combined to form the gain-scheduled controller using the blending functions $\alpha_j(\mu)$, $j = 1,2,3,4$, shown in Figure 13.

The output of each of the transfer functions used to design the fixed-order $\mathscr{H}_\infty$ controller is the deviation of the hub normal force from the nominal value. Using the hub normal force, instead of the deviation of the hub normal force from the nominal value, as the feedback signal will cause a static offset of the trailing edge flaps in our controller implementation. A direct feed-through term in the controller is used to negate the trailing edge flap static offset, by ensuring that the fixed-order $\mathscr{H}_\infty$ controllers all have zero DC gain. The fixed-order $\mathscr{H}_\infty$ controller designed for the advance ratio $\mu = \mu_j$ with the direct feed-through term is denoted by $\widehat{K}_j(s)$, and it has the state-space realization

$$\widehat{K}_j(s) \sim \left(\begin{array}{c|c} A_{k_j} & B_{k_j} \\ \hline C_{k_j} & D_{k_j} \end{array} \right) \tag{28}$$

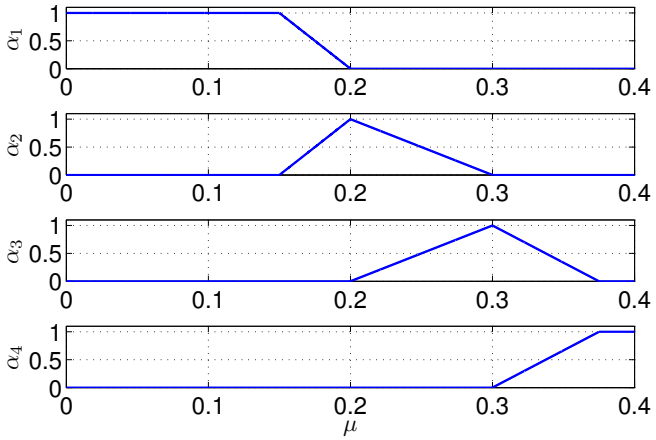

Fig. 13: Blending functions used for the gain-scheduling controller

Table 3: Flight schedules for the closed-loop CAMRAD simulations, $C_T/\sigma = 0.075$

Flight Schedule	Starting μ	Final μ	Duration (sec)
1	0.15	0.2	4
2	0.15	0.3	12
3	0.15	0.375	18

where A_{k_j}, B_{k_j}, C_{k_j} are the state-space matrices of the fixed-order $\mathscr{H}_\infty$ controller $K_j(s)$, and the direct feed-through term D_{k_j} is obtained as

$$D_{k_j} = -K_j(0) \tag{29}$$

The D_{k_j} terms are interpolated in the gain-scheduled controller using the blending functions $\alpha_j(\mu)$ shown in Figure 13. Alternative ways to eliminate the flap static offset are to incorporate a high-pass filter in the control loop, or feedback the deviation of the hub normal force from the nominal hub normal force.

Closed-loop simulation of the helicopter rotor with the gain-scheduled controller were conducted for three different flight profiles as described in Table 3. The gain-scheduled controller was implemented using Fortran subroutines. The harmonic poles of the controller were prewarped to cancel the effect of the integration routine used by CAMRAD. The advance ratio μ was increased linearly in the CAMRAD simulations starting after four seconds, which allowed the large initial transient hub normal force caused by the direct feed-through term to dissipate. The CAMRAD simulations also continued for three seconds after the final value of μ was reached. Because the inflow in the CAMRAD model was not set up to vary with μ, the simulations were conducted with the swashplate collective adjusted after the advance ratio stopped increasing. The adjustment of the swashplate collective ensured that the average hub normal force remained consistent at the beginning and the end of the simulations.

Closed-Loop Simulation Results

The open-loop and closed-loop simulation results for Flight Schedule 1 are shown in Figure 14. The average hub normal force varied as the advance ratio μ was increased, but the adjustment of the swashplate collective ensured that the final average hub normal force matched the nominal value at the start of the simulation.

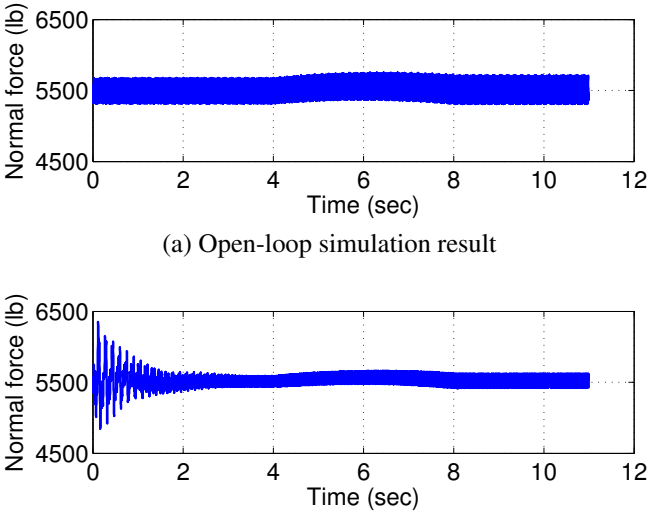

(a) Open-loop simulation result

(b) Closed-loop simulation result

Fig. 14: Open-loop and closed-loop CAMRAD simulation results for Flight Schedule 1, with swashplate collective adjustment

For Flight Schedule 1, the open-loop hub normal force history between $t = 3.8$ sec and $t = 4.2$ sec is shown in Figure 15a, the dominant vibration is at 32.7 Hz, equivalent to 5 per rev. Figure 15b shows the details of the hub normal force between $t = 3.8$ sec and $t = 4.2$ sec for the closed-loop simulation of Flight Schedule 1. The frequency of the dominant vibration is 65.3 Hz, equivalent to 10 per rev, which the gain-scheduled controller was not designed to attenuate. A small amount of the vibration at 5 per rev can be noted in the rise and fall of the successive peaks in the 10 per rev vibration.

Due to the symmetry of the rotor, only harmonic vibrations at multiples of the number of rotor blades (5 per rev, 10 per rev, ...), were present in the simulation. A band-pass filter was used to determine the effectiveness of the gain-scheduled controller at attenuating the vibration at 5 per rev. The band-pass filter consisted of a high-pass Butterworth filter, with a cutoff frequency of 4.5 per rev, in series with a low-pass Butterworth filter, with a cutoff frequency of 5.5 per rev. The band-pass filtered open-loop hub normal force for Flight Schedule 1 is shown in Figure 16a, and the band-pass filtered closed-loop simulation result is shown in Figure 16b. The details of the filtered results between $t = 3.8$ sec and $t = 4.8$ sec are shown in Figure 17. The decrease in the magnitude of the 5 per rev vibration is clearly evident. Within the time span in which μ was increasing, the root mean square (RMS) value of the band-pass filtered normal hub force was attenuated from 103.8 lb to 3.0 lb, a decrease of 97.1%.

For Flight Schedule 2 and Flight Schedule 3, the band-pass filtered CAMRAD simulation results are shown in Figure 18 and Figure 19, respectively. The performance of the gain-scheduled controller in reducing the 5 per rev normal vi-

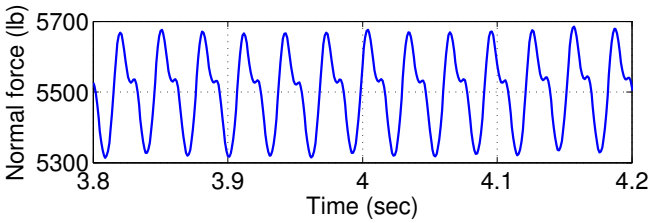

(a) Open-loop simulation result between $t = 3.8$ sec and $t = 4.2$ sec

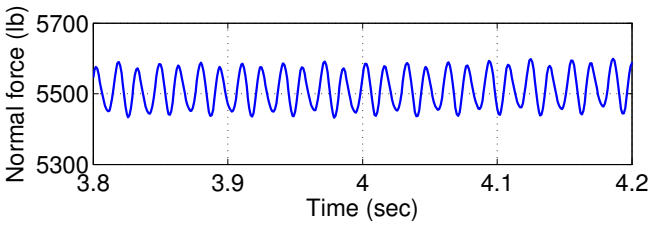

(b) Closed-loop simulation result between $t = 3.8$ sec and $t = 4.2$ sec

Fig. 15: Open-loop and closed-loop CAMRAD simulation results for Flight Schedule 1

Table 4: RMS vibration levels of the band-pass filtered hub normal force during the time span in which μ was increasing

Flight Schedule	Baseline RMS (lb)	Closed-loop RMS (lb)	Reduction (%)
1	103.8	3.0	97.1
2	110.0	2.5	97.7
3	104.9	2.5	97.6

bration is tabulated in Table 4. For all three flight schedules, the controller reduced the RMS value of the band-pass filtered hub normal force by over 97% during the time span in which the advance ratio μ was increasing.

CONCLUSIONS

In this paper, we have presented a method to design a gain-scheduled controller to reduce helicopter vibration throughout the flight envelope. CAMRAD simulation results showed that the rotor dynamics is highly dependent on the advance ratio μ, thus we schedule the controller on μ. We used parametric models derived from the CAMRAD simulation results to design the controller, but our method can be applied to models obtained from windtunnel or flight tests as well. The gain-scheduled controller blends the output signals from fixed-order $\mathscr{H}_\infty$ controllers designed for different values of μ. The specific values of μ are selected to span the entire flight envelope. All of the fixed-order $\mathscr{H}_\infty$ controllers are online throughout the operation, with their signals blended, resulting in bumpless transfer as the flight condition is varied.

The main conclusions from our research are:

1. Analysis of the simulation data showed that the helicopter rotor dynamics is strongly dependent on the advance ratio μ, but only weakly dependent on the rotor shaft angle α, and the blade loading coefficient C_T/σ. The implication is that to achieve high performance full flight envelope harmonic disturbance rejection, the controller must account for the change in the advance ratio during flight.

2. With a simple modification, the fixed-order $\mathscr{H}_\infty$ methodology can be used to design a controller to reduce higher harmonic vibration at different flight conditions, as long as the rotor dynamics do not deviate substantially. The single fixed-order $\mathscr{H}_\infty$ controller is not intended to be used to reduce harmonic vibration at different values of μ. However, the single controller approach appears to be effective when the plant models are at the same value of μ, but different values of the rotor shaft angle α, and blade loading coefficient C_T/σ.

3. The fixed-order $\mathscr{H}_\infty$ controllers can be used in a gain-scheduled controller for full flight envelope vibration reduction. The gain-scheduled controller is scheduled on μ, with the control signal from the fixed-order $\mathscr{H}_\infty$ controllers blended to achieve bumpless transfer. Closed-loop CAMRAD simulations of accelerating forward flights show that the gain-scheduled controller reduced the 5 per rev normal vibration at the rotor hub by over 97%.

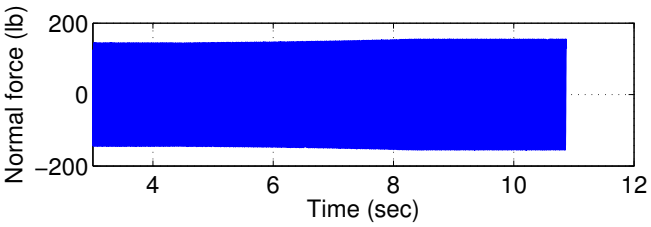

(a) Filtered open-loop simulation result

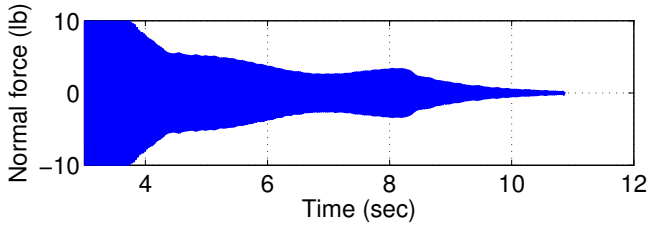

(b) Filtered closed-loop simulation result

Fig. 16: Band-pass filtered open-loop and closed-loop CAMRAD simulation results for Flight Schedule 1

ACKNOWLEDGMENT

This research was funded by the Office of Naval Research, grant number N00014-09-1-0902, with Dr. Judah Milgram serving as the technical monitor. The views expressed in this paper are those of the authors and are not necessarily endorsed by ONR. The authors graciously acknowledge Dr Friedrich Straub of Boeing for providing the CAMRAD simulation results.

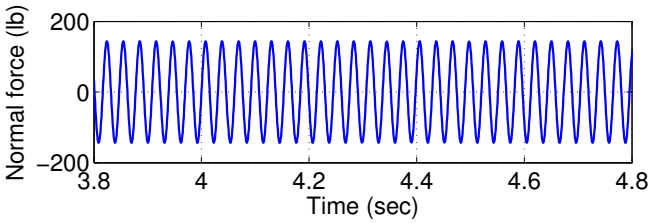

(a) Filtered open-loop simulation result between $t = 3.8$ sec and $t = 4.8$ sec

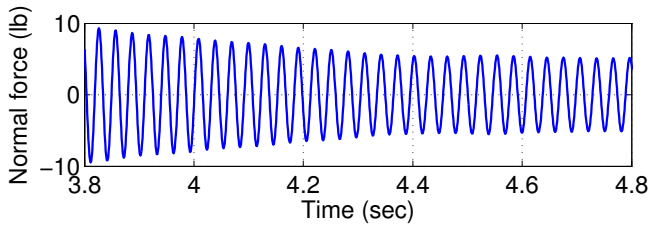

(b) Filtered closed-loop simulation result between $t = 3.8$ sec and $t = 4.8$ sec

Fig. 17: Band-pass filtered open-loop and closed-loop CAMRAD simulation results for Flight Schedule 1

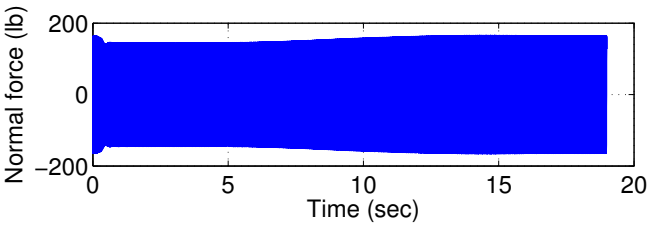

(a) Filtered open-loop simulation result

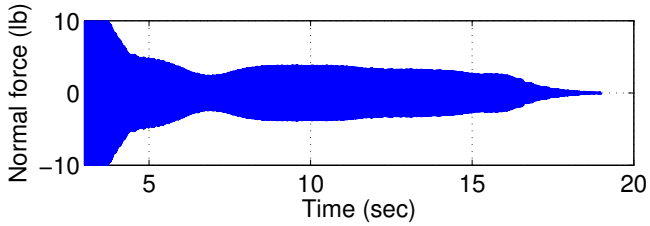

(b) Filtered closed-loop simulation result

Fig. 18: Band-pass filtered open-loop and closed loop CAMRAD simulation results for Flight Schedule 2

REFERENCES

[1]R. W. Du Val, C. Z. Gregory Jr., and N. K. Gupta. Design and Evaluation of a State-Feedback Vibration Controller. *Journal of the American Helicopter Society*, 29(3):30–37, 1984.

[2]F. H. Fan. *Improved Continuous-Time Higher Harmonic Control Using $\mathscr{H}_\infty$ Methods*. PhD thesis, Massachusetts Institute of Technology, 2013.

[3]F. H. Fan and S. R. Hall. An $\mathscr{H}_\infty$ Technique for Improved Higher Harmonic Control. In *Proceedings of the American Helicopter Society 68th Annual Forum*, Fort Worth, TX, May 2012.

[4]B. A. Francis and W. M. Wonham. The Internal Model Principle of Control Theory. *Automatica*, 12(5):457–465, September 1976.

[5]P. P. Friedmann and T. A. Millott. Vibration Reduction in Rotorcraft Using Active Control: A Comparison of Various Approaches. *Journal of Guidance, Control, and Dynamics*, 18(4):664–673, July 1995.

[6]N. K. Gupta. Frequency-Shaped Cost Functionals: Extension of Linear-Quadratic-Gaussian Design Methods. *Journal of Guidance, Control, and Dynamics*, 3(6):529–535, November 1980.

[7]N. K. Gupta and R. W. Du Val. A New Approach for Active Control of Rotorcraft Vibration. *Journal of Guidance, Control, and Dynamics*, 5(2):143–150, March 1982.

[8]S. R. Hall, V. R. Anand, F. K. Straub, and B. H. Lau. Active Flap Control of the SMART Rotor for Vibration Reduction. In *Proceedings of the American Helicopter Society 65th Annual Forum*, Grapevine, TX, May 2009.

[9]S. R. Hall, T. Tzianetopoulou, F. K. Straub, and H. T. Ngo. Design and Testing of a Double X-Frame Piezoelectric Actuator. In *Proceedings of SPIE Smart Structures and Materials*, pages 26–37, Newport Beach, CA, March 2000.

[10]S. R. Hall and N. M. Wereley. Linear Control Issues in the Higher Harmonic Control of Helicopter Vibrations. In *Proceedings of the American Helicopter Society 45th Annual Forum*, Boston, MA, May 1989.

[11]N. D. Ham. Helicopter Individual-Blade-Control and Its Applications. In *Proceedings of the American Helicopter Society 39th Annual Forum*, pages 613–623, St. Louis, MO, 1983.

[12]M. N. Hamouda and G. Pierce. Helicopter Vibration Suppression Using Simple Pendulum Absorbers on the Rotor Blade. *Journal of the American Helicopter Society*, 29(3):19–29, July 1984.

[13]W. Johnson. Self-Tuning Regulators for Multicyclic Control of Helicopter Vibration. *NASA Technical Paper 1996*, March 1982.

[14]L. Ljung. *System Identification*. Prentice Hall, Upper Saddle River, NJ, 1999.

[15]R. G. Loewy. Helicopter Vibrations: A Technological Perspective. *Journal of the American Helicopter Society*, 29(4):4–30, October 1984.

[16]F. McHugh and J. Shaw. Helicopter Vibration Reduction with Higher Harmonic Blade Pitch. *Journal of the American Helicopter Society*, 26(4):26–35, October 1978.

[17]J. A. Molusis, C. E. Hammond, and J. H. Cline. A Unified Approach to the Optimal Design of Adaptive and Gain Scheduled Controllers to Achieve Minimum Helicopter Rotor Vibration. *Journal of the American Helicopter Society*, 28(2):9–18, 1983.

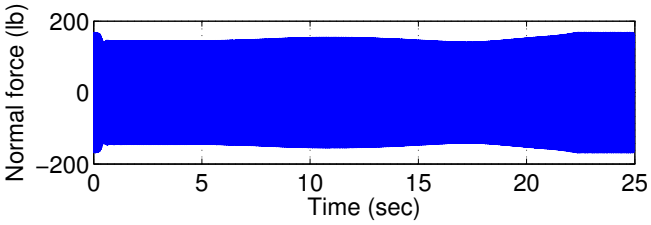

(a) Filtered open-loop simulation result

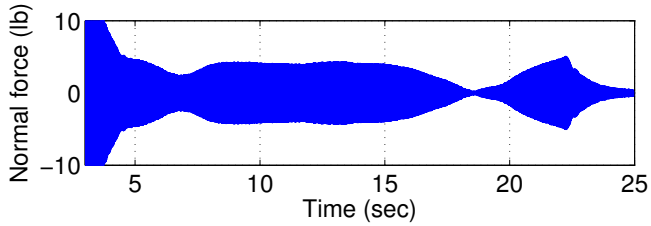

(b) Filtered closed-loop simulation result

Fig. 19: Band-pass filtered open-loop and closed loop CAMRAD simulation results for Flight Schedule 3

[18]J. T. Pearson and R. M. Goodall. Adaptive Schemes for the Active Control of Helicopter Structural Response. *IEEE Transactions on Control Systems Technology*, 2(2):61–72, June 1994.

[19]G. Reichert. Helicopter Vibration Control: A Survey. *Vertica*, 5(1):1–20, 1981.

[20]J. Shaw. Helicopter Vibration Reduction by Higher Harmonic Blade Pitch Control: A Feasibility Study. Master's thesis, Massachusetts Institute of Technology, 1967.

[21]J. Shaw. *Higher Harmonic Blade Pitch Control: A System for Helicopter Vibration Reduction*. PhD thesis, Massachusetts Institute of Technology, 1980.

[22]J. Shaw and N. Albion. Active Control of the Helicopter Rotor for Vibration Reduction. *Journal of the American Helicopter Society*, 26(3):32–39, July 1981.

[23]J. Shaw, N. Albion, E. J. Hanker, and R. S. Teal. Higher Harmonic Control: Wind Tunnel Demonstration of Fully Effective Vibratory Hub Force Suppression. *Journal of the American Helicopter Society*, 34(1):14–25, 1989.

[24]S. Shin, C. E. S. Cesnik, and S. R. Hall. Closed-Loop Control Test of the NASA/Army/MIT Active Twist Rotor for Vibration Reduction. *Journal of the American Helicopter Society*, 50(2):178–194, April 2005.

[25]L. A. Sievers and A. H. von Flotow. Comparison and Extensions of Control Methods for Narrow-Band Disturbance Rejection. *IEEE Transactions on Signal Processing*, 40(10):2377–2391, 1992.

[26]E. R. Wood, R. W. Powers, J. H. Cline, and C. E. Hammond. On Developing and Flight Testing a Higher Harmonic Control System. *Journal of the American Helicopter Society*, 30(1):3–20, 1985.